THE JOURNAL OF PHYSICAL CHEMISTRY A
A JOURNAL OF THE AMERICAN CHEMICAL SOCIETY

pubs.acs.org/JPCA Article

# Enhanced Two-Photon Absorption in Two Triphenylamine-Based All-Organic Compounds

Yu Gong,* Gao-Lei Hou,* Xiangdong Bi,* Narayanan Kuthirummal, Alem Abraha Teklu, Jacob Koenemann, Nico Harris, Peng Wei, Krystal Devera, and Ming Hu*

Cite This: J. Phys. Chem. A 2021, 125, 1870–1879 Read Online

ACCESS | Metrics & More | Article Recommendations | Supporting Information

**ABSTRACT:** Two-photon absorption (TPA) enables the excitation of molecules by comparatively lower energy photons with longer penetration depth and higher spatial precision control, which advances the uses of organic molecules in various applications. In this work, we report two simple all-organic molecules $C_{42}H_{33}N$ (compound **3**) and $C_{138}H_{168}N_4$ (compound **14**) with strong TPA and fluorescent emission activity. Density functional theory calculations show that the enhanced oscillator strengths could be responsible for improved TPA and emission activity for compound **14** compared to those for **3**. The degradation of $C_{138}H_{168}N_4$ under focused laser illumination without circulation is almost negligible within 5 h, making it a candidate for laser dyes. Solid-state measurements confirm the presence of a direct band gap for electron transition that determines the channel to release the absorbed energy and functionality of the studied molecules. This work emphasizes that a high TPA cross-section and selectable energy relaxation (fluorescent emission or heat dissipation) are equally important to the design of advanced functional TPA molecules.

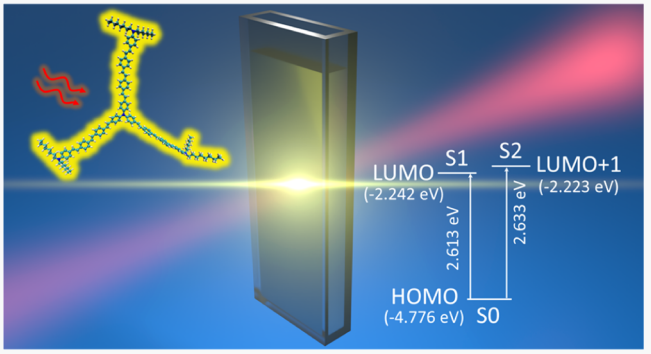




## 1. INTRODUCTION

Organic materials with high intensity of two-photon absorption (TPA) have attracted great interest in recent years, as there is a strong demand for new materials with high TPA cross-sections for a wide range of applications, such as two-photon microscopy,[1−5] microfabrication,[6,7] three-dimensional data storage,[8,9] up-converted lasing,[10,11] and photodynamic therapy.[12−14] Recently, it was reported that human eyes respond to infrared light because of the TPA processes in the retina.[15] Hence, the potential for TPA to enhance the spectrum visibility of human eyes could be expected. TPA is a nonlinear effect, which has the following advantages over the linear effect: (1) absorption in a longer wavelength such as near-infrared range enables better penetration depth in human tissues for microscopy and photodynamic therapy and (2) since the TPA rate is proportional to the square of laser intensity, TPA molecules become soluble or insoluble to the photoresist developer only at the very center of laser focus, which advances the precise operation of microfabrication and three-dimensional data storage.

However, a large TPA cross-section of a material does not necessarily assure its superior performance in the aforementioned applications. From a fundamental physics point of view, the functionality of TPA materials is essentially determined by how they release the absorbed energy, in forms of heat (phonons) or light emission (photons). For example, the applications of lithography and photodynamic therapy require strong phonon generation, while for imaging and lasing, the efficiency of photon emission is more crucial. Therefore, designing organic molecules with superior TPA capability and selective functionalities, which in principle could be realized through manipulation of their configurations, is challenging.[16,17] We feel that controlling the way of energy release is vital to the design of TPA molecules, and it is nontrivial. Molecules with superior performance on both TPA cross-section and heat/photon emission can not only facilitate applications of organic TPA materials but also provide guidance for the optimization of other TPA materials.

Here, we report our results on two simple all-organic molecules that show strong fluorescent emission due to a large TPA cross-section. Density functional theory (DFT) calculations indicate that the enhanced oscillator strengths are responsible for the improved TPA and emission activity for compound **14** compared to those for **3**. The degradation time of these molecules under focused laser excitation is

Received: November 24, 2020
Revised: January 16, 2021
Published: February 26, 2021





https://dx.doi.org/10.1021/acs.jpca.0c10567
J. Phys. Chem. A 2021, 125, 1870–1879

**Scheme 1. Synthesis of TPA Molecule 3**

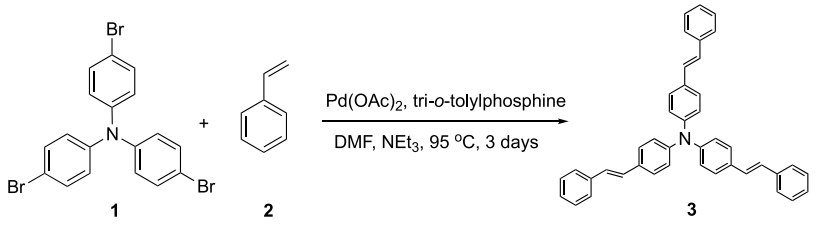


**Scheme 2. Synthesis of TPA Molecule 14**

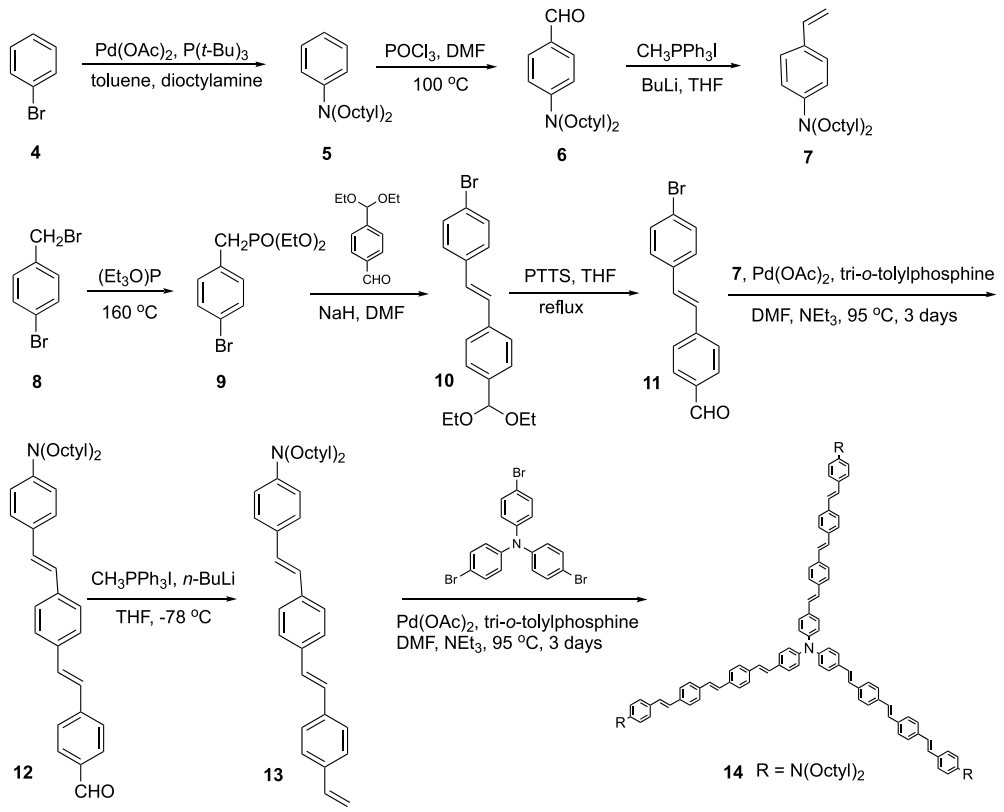


significantly longer than 5−25 h even without circulation and is expected to be much longer than 100 h with the circulation, which is favorable for up-converter lasing applications. Our solid-state characterizations reconfirm the existence of a direct band gap which determines more efficient fluorescent emission than heat dissipation to release the absorbed energy. We expect that the study of superior functional TPA molecules should emphasize on engineering the molecular structure and band gap to achieve an optimal TPA cross-section and most efficient energy relaxation simultaneously.

## 2. METHODS

**2.1. Synthesis and Characterization of TPA Molecule 3.** *2.1.1. (E,E,E)-tris(4-(2-Phenylethenyl)phenyl)amine (3).* Compound **3** (Scheme 1) is prepared by a Heck reaction of tris(4-bromophenyl)amine (**1**) with styrene (**2**) in a 96% yield following a reported procedure.[18] A representative procedure of the Heck reaction is described as given below. Tris(4-bromophenyl)amine (0.482 g, 1 mmol), styrene (0.46 mL, 4 mmol), $Pd(OAc)_2$ (22.4 mg, 0.1 mmol), tri-*o*-tolylphosphine (60.9 mg, 0.2 mmol), $NEt_3$ (0.71 mL, 7.2 mmol), and dimethylformamide (DMF) (2.5 mL) are added to a Schlenk tube equipped with a Teflon valve. Nitrogen is bubbled through the reaction mixture. The reaction tube is sealed and put in an oil bath at 95 °C for 3 days. The reaction mixture is poured into water and is extracted with ethyl acetate (3 × 100 mL). The organic layer is dried over anhydrous $MgSO_4$. Purification of the crude product by column chromatography (silica gel, hexanes/ethyl acetate 10:1) affords the pure product. $^1$H NMR ($CDCl_3$, 250 MHz): $\delta$ 7.06−7.53 (m, 33 H); $^{13}$C NMR ($CDCl_3$, 62.9 MHz): $\delta$ 146.88, 137.72, 132.38, 128.90, 128.22, 127.66, 127.60, 126.54, and 124.46.

**2.2. Synthesis and Characterization of TPA Molecule 14.** *2.2.1. N,N′-Dioctylaniline (5).* Compound **5** (Scheme 2) is synthesized by a C−N coupling reaction of bromobenzene and dioctylamine based on a reported procedure.[19] To a Schlenk tube equipped with a Teflon valve are added bromobenzene (64.7 mg, 0.412 mmol), dioctylamine (109 mg, 0.453 mmol), $Pd(OAc)_2$ (1.7 mg, 0.007 mmol), tri-*t*-butyl phosphine (3 mg, 0.014 mmol), and anhydrous toluene (4 mL). The reaction mixture is degassed and refilled with nitrogen three times. The tube is sealed and heated at 95−110 °C for 2 days. The reaction mixture is poured into water and extracted with ethyl acetate. The crude product is purified by column chromatography (silica gel, hexane/methylene chloride = 1:6) to give the


https://dx.doi.org/10.1021/acs.jpca.0c10567
J. Phys. Chem. A 2021, 125, 1870−1879

pure product (129 mg, yield 99%). $^1$H NMR ($CDCl_3$, 250 MHz): $\delta$ 7.28 (t, 3 H), 6.69 (d, 2 H), 3.32 (t, 4 H), 1.62−1.36 (m, 24 H), and 0.94 (t, 6 H); $^{13}$C NMR ($CDCl_3$, 62.9 MHz): $\delta$ 148.34, 129.40, 115.31, 111.78, 51.26, 32.05, 29.76, 29.56, 27.43, 22.89, and 14.31.

*2.2.2. N,N′-Dioctylaminobenzaldehyde (**6**).* Compound **6** is synthesized by a Veismer reaction of **5** with phosphorus oxychloride to afford the aldehyde functional group following a reported procedure.[20] Phosphorous oxychloride (1.86 mL, 20 mmol) is added dropwise to DMF (7 mL) at 0 °C under nitrogen. The mixture is stirred for 40 min and *N,N*-dioctylaniline (6.34 g, 20 mmol) is added dropwise at room temperature. The reaction mixture is stirred at room temperature for 15 min and then stirred at 110 °C overnight. The reaction is monitored by thin-layer chromatography until no more starting material exists. The reaction mixture is poured into ice water and neutralized by 3 N NaOH solution. The solution is extracted by ethyl acetate. The solvent is evaporated to give a brown oil, which is separated by column chromatography (silica gel, ethyl acetate/hexanes = 1:10) to yield product **6** (6.14 g, yield 89%). $^1$H NMR ($CDCl_3$, 250 MHz): $\delta$ 9.64 (s, 1 H), 7.66 (d, 2 H), 6.61 (d, 2 H), 3.28 (t, 4 H), 1.55−1.25 (m, 24 H), and 0.85 (t, 6 H); $^{13}$C NMR ($CDCl_3$, 62.9 MHz): $\delta$ 189.60, 152.50, 132.08, 124.47, 110.57, 50.99, 31.74, 29.37, 29.25, 27.08, 26.96, 22.58, and 14.04.

*2.2.3. N,N′-Dioctylaminostyrene (**7**).* Compound 7 is synthesized by a Wittig reaction of **6** following a reported procedure.[21] In a nitrogen-filled glovebox, methyltriphenyl phosphonium iodide (8.08 g, 20 mmol) and tetrahydrofuran (THF) (50 mL) are added to a 250 mL round-bottom flask. The flask is taken out of the glovebox and is cooled to −80 °C in a dry ice-acetone bath. A solution of BuLi (1.6 M solution in hexane, 12.5 mL) is added via a syringe under nitrogen. The reaction mixture is allowed to stir at −80 °C for 1 h and then warmed to room temperature for another 1 h period. A solution of 4-*N,N′*-dioctylaminobenzaldehyde (6.9 g, 20 mmol) in 15 mL of THF is added dropwise. The reaction mixture is stirred at room temperature overnight. After the reaction, most of the THF is evaporated and the solution is diluted with hexanes. Most of the salts are removed by filtration. The compound is purified using a basic alumina column yielding product **7** (6.52 g, yield 95%). $^1$H NMR ($CDCl_3$, 250 MHz): $\delta$ 7.43 (d, 2 H), 6.79 (d, 2 H), 5.65 (d, 1 H), 5.12 (d, 1 H), 3.40 (t, 4 H), 1.70−1.44 (m, 24 H), and 1.03 (t, 6 H); $^{13}$C NMR ($CDCl_3$, 62.9 MHz): $\delta$ 147.99, 136.85, 127.50, 125.05, 111.54, 108.55, 51.22, 32.05, 29.72, 29.56, 27.47, 27.35, 22.89, and 14.31.

*2.2.4. (E)-4-(2-(4-Bromophenyl)ethenyl)benzaldehyde Diethyl Acetal (**10**).* Compound **10** is synthesized by a Horner−Wittig reaction of terephthaldehyde monoacetal and 4-bromobenzylbromide with a 57% yield. $^1$H NMR ($CDCl_3$, 250 MHz): $\delta$ 7.50−7.08 (m, 1 0H), 3.72 (m, 4 H), and 1.30 (t, 6 H); $^{13}$C NMR ($CDCl_3$, 62.9 MHz): $\delta$ 138.95, 137.12, 131.96, 130.49, 129.21, 128.51, 128.16, 127.77, 127.26, 126.57, 101.53, 61.20, and 15.40.

*2.2.5. (E)-4-(2-(4-Bromophenyl)ethenyl)benzaldehyde (**11**).* Compound **11** is synthesized based on the modification of a reported procedure.[22] Compound **10** (0.784 g, 2.2 mmol) is dissolved in wet THF (25 mL), and pyridinium tosylate (16.5 mg, 0.66 mmol) is added. The reaction mixture is refluxed for a 1.5 h period. The solvent is removed, and the crude product is purified by column chromatography (silica gel, hexanes/THF = 8:1) to give a pure product (yield 61%). $^1$H NMR ($CDCl_3$, 250 MHz): $\delta$ 10.00 (s, 1 H), 7.90 (d, 2 H), 7.66 (d, 2 H), 7.53 (d, 2 H), 7.43 (d, 2 H), and 7.16 (d, 2 H); $^{13}$C NMR ($CDCl_3$, 62.9 MHz): $\delta$ 191.86, 143.18, 135.65, 132.16, 131.03, 130.45, 128.51, 128.20, 127.15, and 122.53.

*2.2.6. (E,E)-4-(2-(4-(2-(4-Formylphenyl)ethenyl)phenyl)ethenyl)-N,N′-dioctylaniline (**12**).* Compound **12** is synthesized by a Heck cross-coupling reaction of *N,N*-dioctylaminostyrene (**7**) and **11** following the same procedure as for compound 3. (yield 69%).$^1$H NMR ($CDCl_3$, 250 MHz): $\delta$ 10.00 (s, 1 H), 7.90−6.64 (m, 16 H), 3.34 (t, 4 H), 1.62−1.34 (m, 24 H), and 0.95 (t, 6 H); $^{13}$C NMR ($CDCl_3$, 62.9 MHz): $\delta$ 191.97, 148.15, 143.84, 138.99, 135.30, 134.87, 132.23, 130.45, 129.75, 128.12, 127.46, 126.99, 126.49, 125.83, 124.43, 123.03, 111.74, 51.26, 32.05, 29.72, 29.56, 27.51, 27.39, 22.89, and 14.35.

*2.2.7. (E,E)-(2-(4-(2-(4-Dioctylaminophenyl)ethenyl)-phenyl)ethenyl)styrene (**13**).* Compound **13** is synthesized by a Wittig reaction of **12** following the same procedure as for compound **7** (yield 44%). $^1$H NMR ($CDCl_3$, 250 MHz): $\delta$ 7.51−6.62 (m, 16 H), 5.82 (d, 1 H), 5.31 (d, 1 H), 3.32 (t, 4 H), 1.59−1.31 (m, 24 H), and 0.90 (t, 6 H); $^{13}$C NMR ($CDCl_3$, 62.9 MHz): $\delta$ 148.03, 138.09, 137.32, 136.93, 136.70, 135.69, 129.17, 128.66, 128.04, 127.61, 127.03, 126.80, 126.45, 124.59, 123.34, 113.83, 111.78, 51.30, 32.09, 29.76, 29.56, 27.54, 27.39, 22.89, and 14.35.

*2.2.8. (E,E,E,E,E,E,E,E,E)-tris(4-(2-(4-(2-(4-(2-(4-N,N-Dioctylaminophenyl)ethenyl) phenyl)ethenyl)phenyl)-ethenyl)phenyl)amine (**14**).* Compound **14** is prepared by a Heck cross-coupling reaction of tris(4-bromophenyl)amine and **13**. To a Schlenk tube equipped with a Teflon valve are added tris(4-bromophenyl)amine (0.482 g, 1 mmol), **13** (1.918 g, 3.5 mmol), $Pd(OAc)_2$ (22.4 mg, 0.1 mmol), tri-*o*-tolylphosphine (61.2 mg, 0.201 mmol), $Et_3N$ (3 mL, 21.4 mmol), and anhydrous DMF (10 mL). $N_2$ is bubbled through the solution for 5 min, after which the tube is sealed and heated at 100 °C for 3 days. The reaction mixture is poured into water and extracted by methylene chloride. The crude product is purified by column chromatography (silica gel, hexane/methylene chloride = 1:2.5) to give pure product **14** (0.790 g, yield 42%). $^1$H NMR ($CDCl_3$, 250 MHz): $\delta$ 7.50−6.64 (m, 66 H), 3.31 (t, 12 H), 1.59−1.31 (m, 72 H), and 0.93 (t, 18 H); $^{13}$C NMR ($CDCl_3$, 62.9 MHz): $\delta$ 147.99, 146.75, 137.98, 136.89, 136.81, 135.73, 132.39, 129.09, 128.43, 128.04, 127.65, 127.23, 126.99, 126.92, 126.45, 124.59, 124.43, 123.31, 111.78, 51.03, 32.05, 29.68, 29.52, 27.51, 27.35, 22.85, and 14.31; exact mass (1883.2), calculated mass for $C_{138}H_{168}N$ (1882.9). Mass spectrometric peaks are shown at 628.6 and 942.6, corresponding to $(M + 3H)^{3+}$ and $(M + 2H)^{2+}$, respectively (Figure S1).

**2.3. Optical Measurements.** The TPA cross-section is characterized by an open aperture (OA) Z-scan setup.[23] We use an ultrashort laser system (KMLabs Collegiate—Ti:sapphire Laser). This system delivers ultrashort laser pulses with an average power of approximately 650 mW at a repetition rate of 90 MHz. The pulse duration is about 50 fs. The bandwidth, estimated as the full width at half-maximum (fwhm) of the spectrum profile, is 51 nm, and the spectrum is centered at 800 nm. The incident laser power is measured using a digital power meter prior to each measurement before the sample.

The photoacoustic spectra (PAS) are measured using a home-made unit. It is basically an optical absorption spectroscopy technique ideal for studying the optical


https://dx.doi.org/10.1021/acs.jpca.0c10567
J. Phys. Chem. A 2021, 125, 1870−1879

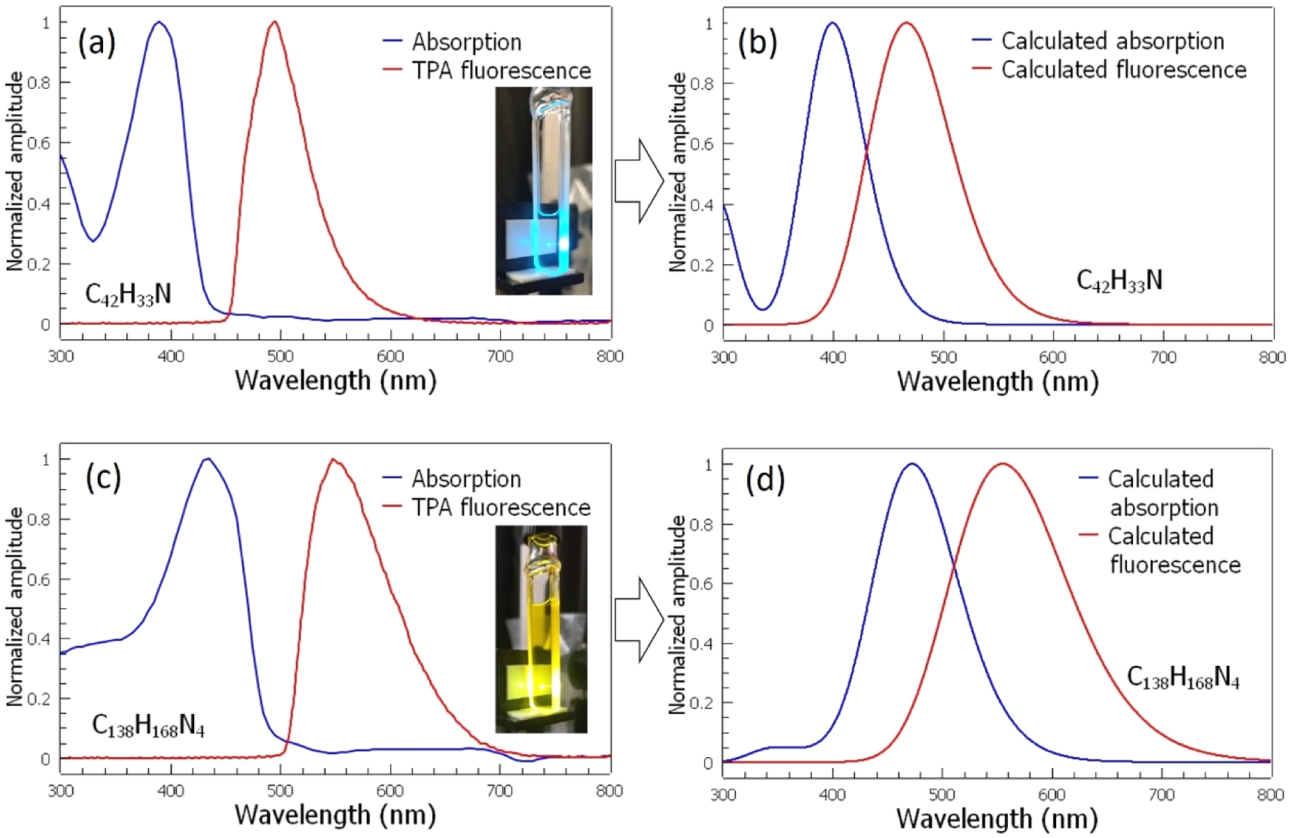


**Figure 1.** Experimental UV−vis absorption and TPA emission spectra of compounds **3** ($C_{42}H_{33}N$) (a) and **14** ($C_{138}H_{168}N_4$) (c) under the excitation of an 800 nm femtosecond laser and their comparison with the simulated ones. Insets of (a,c) are images of TPA fluorescent emission for two molecules with the same concentration.

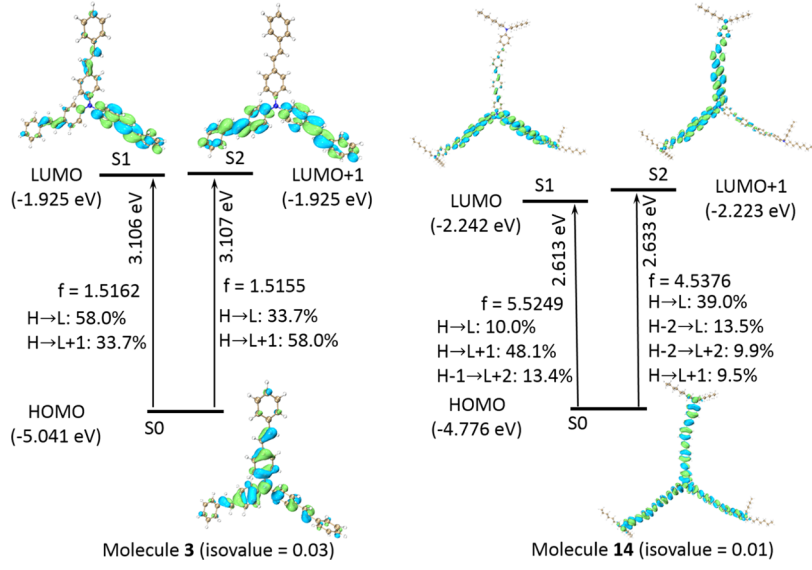


**Figure 2.** Schematic view of the transitions from the ground state (S0) to the first two excited states (S1 and S2) that are nearly degenerate. The transition energies, oscillator strengths, and the mainly involved MOs with their energy levels and contributions to each transition are indicated for both molecules **3** and **14**. Blue and green regions represent the positive and negative orbital phases, respectively. Other involved MOs of molecule **14** are provided in Figure S4 in the Supporting Information.

absorption spectra of opaque and highly light scattering substances such as nanomaterials. In our home-built ultraviolet to visible (UV−vis) PA spectrometer, a light beam from a 300 W Xenon lamp is wavelength-selected using a Cornerstone 260 (1/4 m) monochromator. The wavelength selected beam is intensity-modulated using a variable frequency (47 Hz) mechanical chopper (SRS model SR540). The modulated beam is then focused onto the sample, which is kept in a cell that is airtight and equipped with a 3 Hz to 20 kHz microphone (from Bruel and Kjaer). The signal generated as a


https://dx.doi.org/10.1021/acs.jpca.0c10567
J. Phys. Chem. A 2021, 125, 1870−1879

result of absorption is amplified and then acquired by a lock-in amplifier (SRS Model SR 530). The entire system is controlled through LabVIEW software from National Instruments. Normalization of the PA spectra to a constant input intensity is achieved through the use of a carbon black PA spectrum obtained in the wavelength region of interest.

**2.4. Computational Method.** The ground-state (S0) structures of compounds **3** and **14** are optimized with DFT calculations, and their excited-state structures with time-dependent DFT (TDDFT) are both implemented in the Gaussian09 program package.[24] For the ground-state structures, the B3LYP functional[25,26] with Grimme's dispersion corrections (D3)[27] has been employed, with both def2-SVP and def2-TZVP basis sets[28] having been checked for **3**. Both basis sets give essentially the same geometric structures, molecular orbital (MO) levels, and in particular the highest occupied molecular orbital−lowest unoccupied molecular orbital (HOMO−LUMO) gaps (Table S1 in the Supporting Information). Thus, the def2-SVP basis set was used for all the atoms of **14**, for which the calculation using the def2-TZVP basis set is too expensive. For the excited-state calculations, several functionals including B3LYP,[25,26] PBE0,[29] $\omega$B97XD,[30] and PBE38[27] have been tested to justify their reliability in predicting the excited-state properties. In line with previous findings,[31] the TD-PBE38 functional was found to give the best agreement on calculating the UV−vis and fluorescent emission spectra of **3** compared to the experimental measurement (Figures S2 and S3 in the Supporting Information). Hence, TD-PBE38 was also employed for calculating the excited-state properties of **14**. During the calculations, the self-consistent reaction field method with the polarizable continuum model has been employed to include the solvent effect.[32] We also conducted gas-phase calculations for comparison. The following discussions on computational results have included solvent effects unless otherwise specified.

## 3. RESULTS AND DISCUSSION

**3.1. Experimental UV−Vis Absorption and TPA Emission Spectra.** Figure 1 shows the UV−vis absorption and TPA emission spectra of compounds **3** ($C_{42}H_{33}N$) and **14** ($C_{138}H_{168}N_4$) that are recorded in THF under ambient conditions. It can be seen that the absorption maximums are at 390 and 440 nm for **3** and **14**, respectively. The red shift may be ascribed to the more extensive electron delocalization in **14** with longer arms, resulting in the destabilization of the HOMO (primarily core-based) and stabilization of the LUMO (more localized on the terminal groups of the arms), as shown in Figure 2. No absorption is observed above 550 nm. However, when we apply the femtosecond laser pulse centered at 800 nm to these two molecules, strong bluish and yellowish photon emissions are observed. The compounds **3** and **14** show maximum fluorescent emission features at 500 and 550 nm, respectively (Figure 1). It can be seen that both molecules emit photons with much higher energy than that of the excitation photon (800 nm). Together with the absorption spectra, we conclude that the femtosecond laser pulse-induced fluorescent emission is a nonlinear multiphoton absorption process. In addition, both the absorption and TPA emission bands for **14** are broader than those for **3**, indicating a better TPA efficiency of **14** than that of **3**.

**3.2. Theoretical UV−Vis Absorption and Fluorescent Emission Spectra.** To better understand the measured UV−vis absorption and fluorescent emission spectra, we carried out both DFT and TDDFT calculations on these two molecules. Figure 2 presents the optimized ground-state structures of both molecules and their LUMOs and HOMOs. The plots of HOMOs show that the electron cloud distributes more uniformly across the whole molecule with more extended $\pi$-conjugated benzene rings. Their simulated UV−vis spectra are shown in Figure 1, showing relatively good agreement between the theory and experiment.

The calculations reveal two main transitions, namely, S0 → S1 and S0 → S2, involved in the main absorption peaks of the UV−vis absorption spectra for both molecules **3** and **14**. Figure 2 schematically shows the transition details and the involved MOs. With anticipated more extensive electron delocalization due to more $\pi$-conjugated benzene rings and C═C double bonds in molecule **14**, its HOMO rises in energy (destabilization), while LUMO decreases (stabilization) compared to molecule **3**. In molecule **3**, the electron clouds uniformly distribute on the $\pi$-characterized parts of all the three arms close to the center in its HOMO and more on only one arm in its LUMO and two arms in its LUMO + 1 which is degenerate in energy with LUMO. For molecule **14**, the electron clouds even more uniformly distribute on its three arms except the terminal alkane groups in its HOMO and on two arms in its LUMO and LUMO + 1. Here, it should be noted that with ideally symmetrized geometries for both molecules **3** and **14**, they should have doubly degenerate MOs, that is, LUMO and LUMO + 1 are degenerate. However, due to the large size of the molecules and the flexible end groups with possible rotations, especially for molecule **14**, it is challenging to locate a structure with a perfect symmetry. Those slightly deviated structures will not affect our following analysis. From the MOs, it can be seen that there is more spatial overlap between the occupied and unoccupied orbitals in molecule **14** than that in molecule **3** that contribute to their S0 → S1 and S0 → S2 excitations, resulting in much larger oscillator strengths and stronger adsorption for molecule **14**.

The calculations also show that the S0 → S1 and S0 → S2 transitions essentially have the same energies, in line with that they are both mainly contributed by HOMO to LUMO and LUMO + 1, which are energetically degenerate of molecule **3**. For the S0 → S1 and S0 → S2 excitations of molecule **14**, other orbitals are also involved (Figure 2). In Figure 3, we present the hole−electron analysis as implemented in the Multiwfn software (Version 3.7)[33] to visually understand the nature of electronic excitations for S0 → S1 and S0 → S2, as both involve the contributions from more than a specific pair of MOs.[34] Here, we are focusing on the first excited state (S1) for both molecules **3** and **14** because S1 is normally the critical state to emit fluorescence that plays an important role in the photophysics for closed-shell molecules according to Kasha's rule.[35,36] Note that the S0 → S2 transition is included because S2 is almost degenerate in energy with S1 for both molecules. The hole−electron analysis describes the redistribution of excited electrons, providing a clear picture about the nature of electron excitations. Figure 3 shows that for both molecules and both excitations, the electron only appears on two of the three arms, while the hole appears on all three arms, indicating that the excited electron leaves one arm and arrives at the other two arms. The hole and electron characters of both excitations are very similar and the main difference is which arm only has the hole character. However, compared to molecule **3**, the extent of the hole on the third arm is much less.


https://dx.doi.org/10.1021/acs.jpca.0c10567
J. Phys. Chem. A 2021, 125, 1870−1879

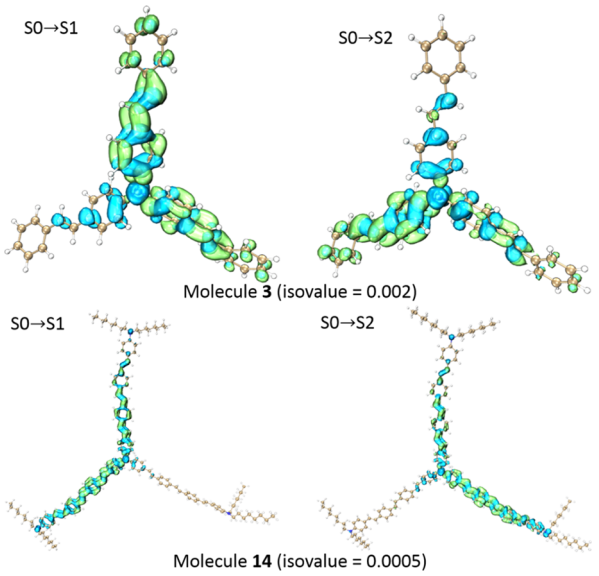


**Figure 3.** Real space representation of hole and electron distributions of molecules **3** and **14** for both S0 → S1 and S0 → S2 excitations. Blue and green regions represent the hole and electron distributions, respectively.

We further analyzed the fluorescent emission properties of both molecules and found that both involve the S1 → S0 transition as expected, with contributions dominated by the LUMO to HOMO for molecule **3** (93.6%) and molecule **14** (88.8%), respectively. Their calculated oscillator strengths (f) are 1.6743 and 4.4083, respectively, and the much larger f value calculated for molecule **14** may explain its enhanced fluorescent emission activity compared to molecule **3**. In addition, based on the Einstein equation,[37] the radiative lifetime for molecule **3** is estimated to be 1.6 ns, and for molecule **14**, it is about 0.6−0.7 ns; this may result in higher emission probability and thus higher emission intensity for molecule **14**.

**3.3. TPA Cross-Sections and Stabilities.** To quantitatively compare the TPA efficiency of the two molecules, we carried out the *Z*-scan experiment in which the transmission of the laser is monitored as a function of sample position when it is passing through the focal point of the lens along the *Z*-direction.[23] Figure 4 shows the normalized OA *Z*-scan transmission results (open squares) for $C_{42}H_{33}N$ and $C_{138}H_{168}N_4$ under the excitation of the 800 nm femtosecond laser. As shown in Figure 4, the transmission gradually decreases to a minimum value as the sample is approaching the focal point of an optical lens (100 mm focal length). This may be ascribed to the nonlinear TPA processes, which depend on the spatial and temporal excitation energy density. At the focal point ($z = 0$), the spatial density of excitation light energy is the highest, and the TPA process reaches maximum (with strongest fluorescent emission), while the 800 nm transmission is minimum. The temporal energy density of the excitation light is guaranteed by 50 fs laser pulses. Even though the sample is far away from the focal point, one can still see fluorescent emission from both molecules. In addition, molecule **14** shows a much lower transmission value of ∼0.55 compared to that of molecule **3** (∼0.87) at $z = 0$. This indicates a higher TPA efficiency for molecule **14**, or more common, larger TPA cross-section $\sigma$. TPA can be described by the relation[38]

$$-\frac{dI}{dz} = \alpha I + \beta I^2 \tag{1}$$

where $\alpha$ is the linear (one photon) absorption coefficient (in our case $\alpha \sim 0$) and $\beta$ is the TPA coefficient. In addition, $\beta = N/E\sigma$, in which $N$ is the number density of molecules in units of $cm^{-3}$ (2 mM in the current case), $E$ is the photon energy in Joule, and $\sigma$ is the TPA cross-section ($cm^4 \cdot s \cdot molecule^{-1} \cdot photon^{-1}$; 1 GM = $10^{-50}$ $cm^4 \cdot s \cdot molecule^{-1} \cdot photon^{-1}$). The TPA coefficient $\beta$ can be extracted from numerical fitting of normalized OA *Z*-scan transmission, which is described by[23]

$$T(z) = \sum_{n=0}^{\infty} \frac{-q_0^{\,n}}{(n+1)^{3/2}(1 + {}^{z}/_{z_0}{}^{2})^n} \tag{2}$$

where

$q_0 = \beta L_{\text{eff}} I_0$, and $L_{\text{eff}} = \frac{1 - e^{-\alpha L}}{\alpha} \sim L(0.1\ \text{cm})$ when $\alpha \sim 0$. $I_0$ is the maximum on-axis intensity in the focus. For a Gaussian beam, $I_0$ is given by

$$I_0 = \frac{2P_{\text{average}}}{\pi \omega_0^{\,2} R \tau} \tag{3}$$

where $P_{\text{average}}$ is the average input laser power, $\omega_0$ is the beam waist radius, $R$ is the pulse repetition rate, and $\tau$ is the pulse width. In the current case, $P_{\text{average}}$ = 450 mW, $\tau$ = 50 fs, $R$ = 90 MHz, and $\omega_0$ is estimated to be 33.9 $\mu$m, which gives a maximum on-axis intensity in the focus $I_0 \sim 5.5$ GW/cm$^2$. Combining with the fitting of *Z*-scan results in Figure 4, we

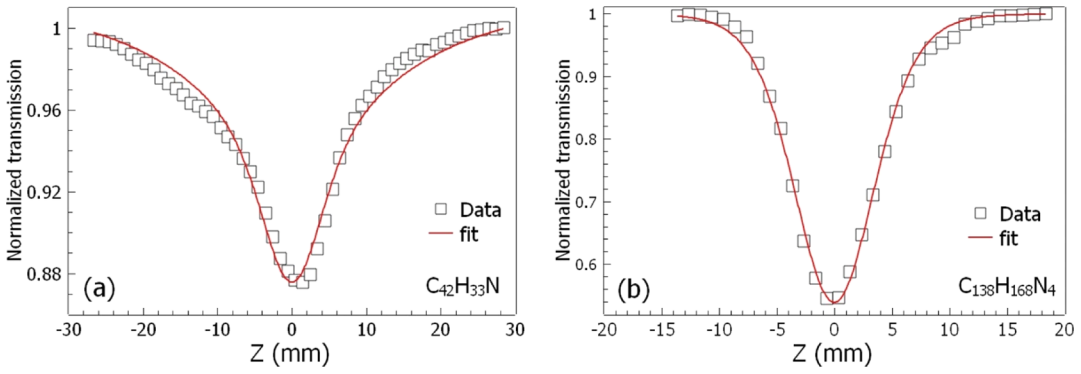


**Figure 4.** Normalized OA Z-scan transmission (open squares) and fit (red solid line) for $C_{42}H_{33}N$ (a) and $C_{138}H_{168}N_4$ (b) under the excitation of the femtosecond laser (50 fs width pulses, wavelength centered at 800 nm).



https://dx.doi.org/10.1021/acs.jpca.0c10567
J. Phys. Chem. A 2021, 125, 1870−1879

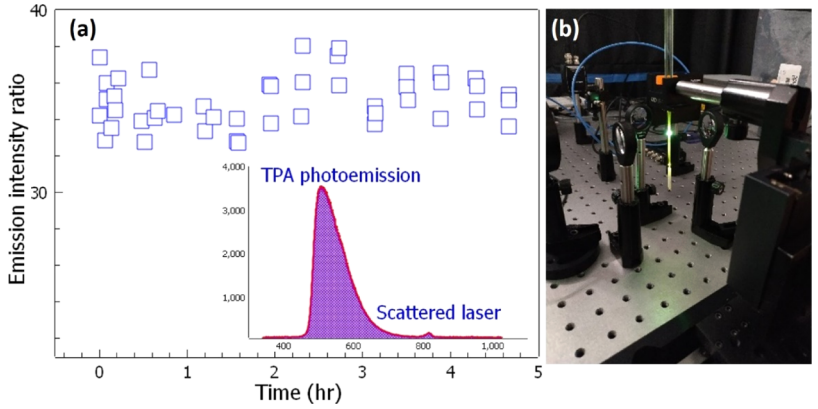


**Figure 5.** Degradation for $C_{138}H_{168}N_4$ under laser illumination. (a) Intensity ratio between TPA fluorescent emission and scattered laser in the spectrum plotted as a function of time for about 5 h. The inset shows the typical spectrum including TPA fluorescent emission and a scattered pump laser. The measurement setup is shown in (b).

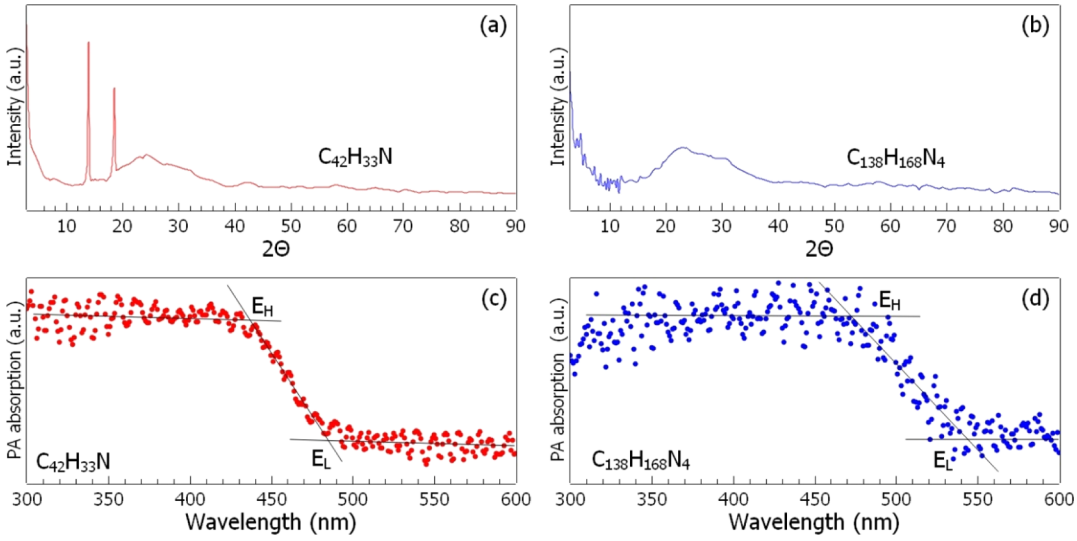


**Figure 6.** XRD patterns for $C_{42}H_{33}N$ (a) and $C_{138}H_{168}N_4$ (b) thin films and their room-temperature PA spectra (c,d).

determined the TPA cross-sections to be $1.3 \times 10^4$ GM for molecule **3** and $5.3 \times 10^4$ GM for molecule **14**. For relatively simple molecules, the TPA cross-sections are comparatively large.[39] The fluorescence quantum yield of $C_{138}H_{168}N_4$ is characterized to be around 2%, which is about 3 times larger than that of $C_{42}H_{33}N$.

One important application of the multiphoton absorption materials is to achieve frequency upconversion of coherent light. Most commonly used strategies for frequency upconversion are sum-frequency or high harmonic generation in nonlinear crystals. In order to obtain high conversion efficiency, critical phase-matching is needed but that is normally challenging to achieve only if sophisticated techniques such as birefringence in crystals or anomalous dispersion in isotropic materials are employed. In contrast, multiphoton lasing can be achieved without a phase-matching requirement in liquid or solid materials.[40−42] In particular, multiphoton lasing in dye-based systems owns the advantage of large tunability within a relatively broad spectral range. However, lasing dyes usually suffer from the degradation of dye molecules under the pump laser illumination.[43] Hence, we investigated the degradation of molecule **14** under pump laser illumination. We monitored TPA fluorescent emission intensity for about 5 h. Considering the laser power-induced TPA fluorescent emission variation during long-time operation, we plot in Figure 5a the ratio of TPA fluorescent emission intensity and scattered pump laser intensity from the fluorescent emission spectrum (a typical spectrum is shown in the inset of Figure 5a). The setup is shown in Figure 5b, and the pump laser is focused into a glass pipette filled with solvent. The fluorescent emission (as well as scattered pump laser) is collected perpendicularly to the pump laser by a converging lens into a spectrometer. After 5 h operation without circulation, the intensity ratio shows no obvious decrease, which implies almost no drop of the TPA fluorescent emission intensity. We thus conclude that the TPA molecule is stable even without circulation under pump laser excitation. Due to photodissociation by the pump laser, laser dyes usually start to degrade within 5−25 h[44] Hence, the stability of our designed molecule makes it promising in the application of long-operation upper conversion dye lasers. Further test for longer operation experiments could be carried out to evaluate its stability under pump laser excitation.

**3.4. Solid-State Property.** In addition to characterizing the two TPA molecules in the THF solution, we also examined their solid-state films. The solid-state films were prepared by drop-coating of the molecule in THF solutions on a clean glass substrate (THF evaporates afterward). Figure 6 presents the X-


https://dx.doi.org/10.1021/acs.jpca.0c10567
J. Phys. Chem. A 2021, 125, 1870−1879

ray diffractions (XRDs) for the two molecules. Sharp diffraction peaks are observed in the $C_{42}H_{33}N$ XRD spectrum, while no diffraction peaks are observed for $C_{138}H_{168}N_4$. The broad background hump in the spectra is from the glass substrate,[45] while the sharp peaks are from polycrystallized $C_{42}H_{33}N$ molecules. We have made separately two samples to confirm the diffraction peaks. From the fwhm of diffraction peaks, we estimate the crystal grain size in the thin film of molecule **3** to be about 32 nm. Normally, the films of large-size all-organic molecules are amorphous,[46] and no sharp peak has been observed in the XRD spectrum of compound **14**. Although the fundamental understanding of the crystallization of all-organic material is not yet fully achieved,[47] organic thin films have been used in many applications. For example, similar organic molecules have been successfully integrated into perovskite solar cells as a hole-transporting layer which plays a key role in facilitating hole transport from the perovskite to the back contact and inhibiting back electron transfer.[48,49] Exploring thin-film organic semiconductors has been an essential requirement in the development of organic semiconductor devices.[50,51] We here employed the PA absorption measurements to explore their semiconductor properties.[52] As shown in Figure 6, both samples show typical step-shape spectra, indicating that the two molecules are semiconductors in their solid-state forms. Using the method utilized to analyze the band gap,[53,54] we determine two characteristic edges, $E_H$ and $E_L$, present in the PA spectra for both molecules. Then the band gap position is determined as $E_g^{PA} = (E_L + E_H)/2 = 2.69$ eV for $C_{42}H_{33}N$ and 2.44 eV for $C_{138}H_{168}N_4$. These band gap values correspond to the leading edge of TPA fluorescent emission of the two molecules, which suggest that these are direct band gaps.

Of the studied molecules, the tuning of the band gap with a slightly modified molecular structure allows for controlling the fluorescent emission wavelength, while a large TPA cross-section is still maintained. It is expected that further modification of the molecular structure may shift the emission wavelength from the visible to the infrared region until the band gap is low enough to make nonradiative decay processes to dominate over radiative fluorescent emission.[55] In addition, since the application of the TPA material is determined by both efficient TPA absorption and subsequent energy-releasing processes, such as fluorescent emission, we aim to further enhance the fluorescent emission efficiency based on our TPA molecules. For example, a previous study showed that changing the functional groups from carboxylic to sulfonic acid not only enables high water solubility but also dramatically enhances fluorescent emission efficiency.[56] Our follow-up study will focus on modifying the functional group to enhance the fluorescent emission efficiency while monitoring the TPA cross-section. It is also expected that by further engineering the morphology and manipulating the band gap, the studied molecules could be potentially integrated into all-organic semiconductor devices such as logic and sensors.[57]

## 4. CONCLUSIONS

In summary, we have studied the fluorescent emission and TPA properties of two simple all-organic molecules. DFT calculations indicate that the improved TPA and emission activity may stem from the enhanced oscillator strengths associated with the ground-/excited-state transitions in the two molecules. The degradation time of compound **14** under focused laser excitation is longer than 5−25 h without circulation and is expected to be much longer than 100 h with circulation. Both molecules are nontoxic and noncorrosive, making them favorable for up-converter lasing applications. We further emphasize that the application of TPA materials is crucially dependent on both TPA and efficient energy-releasing processes (fluorescent emission or heat dissipation). Solid-state characterizations confirm a direct band gap in the visible range, which enables more efficient fluorescent emission than nonradiative decay in our designed molecules to release the TPA energy. Therefore, engineering the molecular structure and band gap for efficient TPA and energy-releasing processes need to be considered equivalently to design novel functional TPA molecules. Since our molecules are nontoxic and noncorrosive, it is expected that the developed molecular system may address the future needs for environmentally friendly and biocompatible TPA materials.

## ■ ASSOCIATED CONTENT

### Supporting Information

The Supporting Information is available free of charge at https://pubs.acs.org/doi/10.1021/acs.jpca.0c10567.

Further details on the geometric structures and MO levels, LC−MS spectrum of compound 14, comparison of the simulated UV−vis absorption spectra and fluorescence spectra as well as the MOs and their energy levels that contribute to the S0 → S1 and S0 → S2 transitions for compound 14, and cartesian coordinates of compounds 3 and 14 (PDF)

## ■ AUTHOR INFORMATION


### Corresponding Authors

**Yu Gong** − *Department of Physics and Astronomy, College of Charleston, Charleston 29407, South Carolina, United States;* orcid.org/0000-0002-9357-9503; Email: gongy@cofc.edu

**Gao-Lei Hou** − *Quantum Solid-State Physics, Department of Physics and Astronomy, KU Leuven, Leuven 3001, Belgium;* orcid.org/0000-0003-1196-2777; Email: gaolei.hou@kuleuven.be, chemglhou@gmail.com

**Xiangdong Bi** − *Department of Chemistry, Charleston Southern University, Charleston 29485, South Carolina, United States;* Email: Xbi@csuniv.edu

**Ming Hu** − *Department of Mechanical Engineering, University of South Carolina, Columbia 29208, South Carolina, United States;* orcid.org/0000-0002-8209-0139; Email: HU@sc.edu

### Authors

**Narayanan Kuthirummal** − *Department of Physics and Astronomy, College of Charleston, Charleston 29407, South Carolina, United States*

**Alem Abraha Teklu** − *Department of Physics and Astronomy, College of Charleston, Charleston 29407, South Carolina, United States*

**Jacob Koenemann** − *Department of Physics and Astronomy, College of Charleston, Charleston 29407, South Carolina, United States*

**Nico Harris** − *Department of Physics and Astronomy, College of Charleston, Charleston 29407, South Carolina, United States*

**Peng Wei** − *Affinity Research Chemicals, Inc., Wilmington 19804, Delaware, United States*

**Krystal Devera** − *Department of Physics and Astronomy, College of Charleston, Charleston 29407, South Carolina, United States*

Complete contact information is available at: https://pubs.acs.org/10.1021/acs.jpca.0c10567

### Notes

The authors declare no competing financial interest.

## ■ ACKNOWLEDGMENTS

The authors would like to thank Dr. Jay Forsythe from Chemistry and Biochemistry Department (College of Charleston) for his help with the UV−vis measurements. Research reported in this publication was supported in part by the NSF and SC EPSCoR/IDeA (MADE in SC) Program under NSF award #OIA-1655740 and GEAR CRP 20-GC02. The views, perspective, and content do not necessarily represent the official views of the SC EPSCoR Program or those of the NSF.

## ■ REFERENCES

(1) Kim, H. M.; Cho, B. R. Small-molecule Two-photon Probes for Bioimaging Applications. *Chem. Rev.* **2015**, *115*, 5014−5055.
(2) Park, Y. I.; Lee, K. T.; Suh, Y. D.; Hyeon, T. Upconverting Nanoparticles: A Versatile Platform for Wide-Field two-Photon Microscopy and Multi-Modal in Vivo Imaging. *Chem. Soc. Rev.* **2015**, *44*, 1302−1317.
(3) Niu, W.; Guo, L.; Li, Y.; Shuang, S.; Dong, C.; Wong, M. S. Highly Selective Two-Photon Fluorescent Probe for Ratiometric Sensing and Imaging Cysteine in Mitochondria. *Anal. Chem.* **2016**, *88*, 1908−1914.
(4) Li, J.; Cheng, F.; Huang, H.; Li, L.; Zhu, J.-J. Nanomaterial-based Activatable Imaging Probes: From Design to Biological Applications. *Chem. Soc. Rev.* **2015**, *44*, 7855−7880.
(5) Yuan, L.; Wang, L.; Agrawalla, B. K.; Park, S.-J.; Zhu, H.; Sivaraman, B.; Peng, J.; Xu, Q.-H.; Chang, Y.-T. Development of Targetable Two-photon Fluorescent Probes to Image Hypochlorous Acid in Mitochondria and Lysosome in Live Cell and Inflamed Mouse Model. *J. Am. Chem. Soc.* **2015**, *137*, 5930−5938.
(6) LaFratta, C. N.; Fourkas, J. T.; Baldacchini, T.; Farrer, R. A. Multiphoton Fabrication. *Angew. Chem., Int. Ed. Engl.* **2007**, *46*, 6238−6258.
(7) Teran, N. B.; He, G. S.; Baev, A.; Shi, Y.; Swihart, M. T.; Prasad, P. N.; Marks, T. J.; Reynolds, J. R. Twisted Thiophene-Based Chromophores with Enhanced Intramolecular Charge Transfer for Cooperative Amplification of Third-Order Optical Nonlinearity. *J. Am. Chem. Soc.* **2016**, *138*, 6975−6984.
(8) Yu, J.; Cui, Y.; Xu, H.; Yang, Y.; Wang, Z.; Chen, B.; Qian, G. Confinement of pyridinium hemicyanine dye within an anionic metal-organic framework for two-photon-pumped lasing. *Nat. Commun.* **2013**, *4*, 2719.
(9) Yu, J.; Cui, Y.; Wu, C.-D.; Yang, Y.; Chen, B.; Qian, G. Two-photon Responsive Metal-organic Framework. *J. Am. Chem. Soc.* **2015**, *137*, 4026−4029.
(10) Huang, B. Native Point Defects in CaS: Focus on Intrinsic Defects and Rare Earth Ion Dopant Levels for Up-converted Persistent Luminescence. *Inorg. Chem.* **2015**, *54*, 11423−11440.
(11) Lin, T. C.; Chung, S. J.; Kim, K. S.; Wang, X.; He, G. S.; Swiatkiewicz, J.; Prasad, P. N. Organics and Polymers with High Two-Photon Activities and their Applications. *Advances in Polymer Science*; Springer Nature, 2003; Vol. *161*, pp 157−193.
(12) Lu, K.; He, C.; Lin, W. A Chlorin-Based Nanoscale Metal-Organic Framework for Photodynamic Therapy of Colon Cancers. *J. Am. Chem. Soc.* **2015**, *137*, 7600−7603.
(13) Zeng, C.; Shang, W.; Liang, X.; Liang, X.; Chen, Q.; Chi, C.; Du, Y.; Fang, C.; Tian, J. Cancer Diagnosis and Imaging-Guided Photothermal Therapy Using a Dual-Modality Nanoparticle. *ACS Appl. Mater. Interfaces* **2016**, *8*, 29232−29241.
(14) Chen, G.; Roy, I.; Yang, C.; Prasad, P. N. Nanochemistry and Nanomedicine for Nanoparticle-based Diagnostics and Therapy. *Chem. Rev.* **2016**, *116*, 2826−2885.
(15) Artal, P.; Manzanera, S.; Komar, K.; Gambín-Regadera, A.; Wojtkowski, M. Visual Acuity in Two-photon Infrared Vision. *Optica* **2017**, *4*, 1488.
(16) Albota, M.; Beljonne, D.; Brédas, J. L.; Ehrlich, J. E.; Fu, J. Y.; Heikal, A. A.; Hess, S. E.; Kogej, T.; Levin, M. D.; Marder, S. R.; et al. Design of Organic Molecules with Large Two-photon Absorption Cross Sections. *Science* **1998**, *281*, 1653−1656.
(17) Liu, Z.; Lu, T. Optical Properties of Novel Conjugated Nanohoops: Revealing the Effects of Topology and Size. *J. Phys. Chem. C* **2020**, *124*, 7353−7360.
(18) Meier, H.; Hanold, N.; Kalbitz, H. Synthesis of Hexastyrylbenzenes. *Synthesis* **1997**, *1997*, 276.
(19) Watanabe, M.; Nishiyama, M.; Yamamoto, T.; Koie, Y. Palladium/P(t-Bu)3-catalyzed synthesis of N-aryl azoles and application to the synthesis of 4,4′,4″-tris(N-azolyl)triphenylamines. *Tetrahedron Lett.* **2000**, *41*, 481.
(20) Lai, G.; Bu, X.; Santos, J.; Mintz, E. Reinvestigation of the Vilsmeier-Haack Formylation of Triphenylamine. *Synlett* **1997**, *1997*, 1275−1276.
(21) Tew, G. N.; Pralle, M. U.; Stupp, S. I. Supramolecular Materials with Electroactive Chemical Functions. *Angew. Chem., Int. Ed. Engl.* **2000**, *39*, 517−521.
(22) Sterzycki, R. Pyridinium Tosylate, A Mild Catalyst for Formation and Cleavage of Dioxolane-Type Acetals. *Synthesis* **1979**, *1979*, 724−725.
(23) Sheik-Bahae, M.; Said, A. A.; Wei, T.-H.; Hagan, D. J.; Van Stryland, E. W. Sensitive Measurement of Optical Nonlinearities Using a Single Beam. *IEEE J. Quantum Electron.* **1990**, *26*, 760−769.
(24) Frisch, M. J.; Trucks, G. W.; Schlegel, H. B.; Scuseria, G. E.; Robb, M. A.; Cheeseman, J. R.; Scalmani, G.; Barone, V.; Petersson, G. A.; Nakatsuji, H.; et al. *Gaussian 09*, Revision E.01, Gaussian, Inc.: Wallingford CT, 2013.
(25) Lee, C.; Yang, W.; Parr, R. G. Development of the Colle-Salvetti Correlation-energy Formula into a Functional of the Electron Density. *Phys. Rev. B: Condens. Matter Mater. Phys.* **1988**, *37*, 785−789.
(26) Becke, A. D. Density-functional Thermochemistry. III. The Role of Exact Exchange. *J. Chem. Phys.* **1993**, *98*, 5648−5652.
(27) Grimme, S.; Antony, J.; Ehrlich, S.; Krieg, H. A Consistent and Accurate AB Initio Parametrization of Density Functional Dispersion Correction (DFT-D) for the 94 Elements H-Pu. *J. Chem. Phys.* **2010**, *132*, 154104.
(28) Weigend, F.; Ahlrichs, R. Balanced Basis Sets of Split Valence, Triple Zeta Valence and Quadruple Zeta Valence Quality for H to Rn: Design and Assessment of Accuracy. *Phys. Chem. Chem. Phys.* **2005**, *7*, 3297−3305.
(29) Adamo, C.; Barone, V. Toward Reliable Density Functional Methods without Adjustable Parameters: The PBE0 Model. *J. Chem. Phys.* **1999**, *110*, 6158−6170.
(30) Chai, J.-D.; Head-Gordon, M. Long-range Corrected Hybrid Density Functionals with Damped Atom-atom Dispersion Corrections. *Phys. Chem. Chem. Phys.* **2008**, *10*, 6615−6620.
(31) Goerigk, L.; Grimme, S. A Thorough Benchmark of Density Functional Methods for General Main Group Thermochemistry, Kinetics, and Noncovalent Interactions. *Phys. Chem. Chem. Phys.* **2011**, *13*, 6670−6688.
(32) Tomasi, J.; Mennucci, B.; Cammi, R. Quantum Mechanical Continuum Solvation Models. *Chem. Rev.* **2005**, *105*, 2999−3094.
(33) Lu, T.; Chen, F. Multiwfn: A Multifunctional Wavefunction Analyzer. *J. Comput. Chem.* **2012**, *33*, 580−592.
(34) Liu, Z.; Lu, T.; Chen, Q. An Sp-hybridized All-carboatomic Ring, Cyclo[18]carbon: Electronic Structure, Electronic Spectrum, and Optical Nonlinearity. *Carbon* **2020**, *165*, 461−467.

(35) Kasha, M. Characterization of Electronic Transitions in Complex Molecules. *Discuss. Faraday Soc.* **1950**, *9*, 14−19.
(36) del Valle, J. C.; Catalán, J. Kasha's Rule: A Reappraisal. *Phys. Chem. Chem. Phys.* **2019**, *21*, 10061−10069.
(37) Chaitanya, K.; Ju, X.-H.; Heron, B. M. Theoretical Study on the Light Harvesting Efficiency of Zinc Porphyrin Sensitizers for DSSCs. *RSC Adv.* **2014**, *4*, 26621−26634.
(38) Bass, M. *Handbook of Optics: Fundamentals, Techniques, and Design*; McGraw-Hill, 1994; Vol. *1*.
(39) He, G. S.; Tan, L.-S.; Zheng, Q.; Prasad, P. N. Multiphoton Absorbing Materials: Molecular Designs, Characterizations, and Applications. *Chem. Rev.* **2008**, *108*, 1245−1330.
(40) He, G. S.; Markowicz, P. P.; Lin, T.-C.; Prasad, P. N. Observation of Stimulated Emission by Direct three-photon Excitation. *Nature* **2002**, *415*, 767−770.
(41) He, G. S.; Lin, T.-C.; Chung, S.-J.; Zheng, Q.; Lu, C.; Cui, Y.; Prasad, P. N. Two-, Three-, and Four-photon-pumped Stimulated Cavityless Lasing Properties of Ten Stilbazolium-dyes Solutions. *J. Opt. Soc. Am. B* **2005**, *22*, 2219−2228.
(42) Markowicz, P. P.; He, G. S.; Prasad, P. N. Direct Four-photon Excitation of Amplified Spontaneous Emission in A Nonlinear Organic Chromophore. *Opt. Lett.* **2005**, *30*, 1369−1371.
(43) Fletcher, A. N. Laser Dye Stability. *Appl. Phys. B* **1983**, *31*, 19−26.
(44) Ready, J. F. *Industrial Applications of Lasers*; Elsevier, 1997; p 599.
(45) Chakraborty, R.; Dey, A.; Mukhopadhyay, A. K. Loading Rate Effect on Nanohardness of Soda-Lime-Silica Glass. *Metall. Mater. Trans. A* **2010**, *41*, 1301−1312.
(46) Kuila, S.; Garain, S.; Bandi, S.; George, S. J. All-Organic, Temporally Pure White Afterglow in Amorphous Films Using Complementary Blue and Greenish-Yellow Ultralong Room Temperature Phosphors. *Adv. Funct. Mater.* **2020**, *30*, 2003693.
(47) Tsarfati, Y.; Rosenne, S.; Weissman, H.; Shimon, L. J. W.; Gur, D.; Palmer, B. A.; Rybtchinski, B. Crystallization of Organic Molecules: Nonclassical Mechanism Revealed by Direct Imaging. *ACS Cent. Sci.* **2018**, *4*, 1031−1036.
(48) Zhao, X. M.; Zhang, F.; Yi, C. Y.; Bi, D. Q.; Bi, X. d.; Wei, P.; Luo, J.; Liu, X. C.; Wang, S. R.; Li, X. G.; et al. A Novel One-step Synthesized and Dopant-free Hole Transport Material for Efficient and Stable Perovskite Solar Cells. *J. Mater. Chem. A* **2016**, *4*, 16330−16334.
(49) Zhang, F.; Yi, C.; Wei, P.; Bi, X.; Luo, J.; Jacopin, G.; Wang, S.; Li, X.; Xiao, Y.; Zakeeruddin, S. M.; et al. A Novel Dopant-Free Triphenylamine Based Molecular "Butterfly" Hole-Transport Material for Highly Efficient and Stable Perovskite Solar Cells. *Adv. Energy Mater.* **2016**, *6*, 1600401.
(50) Newman, C. R.; Frisbie, C. D.; da Silva Filho, D. A.; Brédas, J.-L.; Ewbank, P. C.; Mann, K. R. Introduction to Organic Thin Film Transistors and Design of n-Channel Organic Semiconductors. *Chem. Mater.* **2004**, *16*, 4436−4451.
(51) Zeidell, A. M.; Jennings, L.; Frederickson, C. K.; Ai, Q.; Dressler, J. J.; Zakharov, L. N.; Risko, C.; Haley, M. M.; Jurchescu, O. D. Organic Semiconductors Derived from Dinaphtho-Fused s-Indacenes: How Molecular Structure and Film Morphology Influence Thin-Film Transistor Performance. *Chem. Mater.* **2019**, *31*, 6962−6970.
(52) Kuthirummal, N. Listening to Nanomaterials: Photoacoustic Spectroscopy. *J. Chem. Educ.* **2009**, *86*, 1238.
(53) Zelewski, S. J.; Kudrawiec, R. Photoacoustic and Modulated Reflectance Studies of Indirect and Direct Band Gap in van der Waals Crystals. *Sci. Rep.* **2017**, *7*, 15365.
(54) Prías-Barragán, J. J.; Tirado-Mejía, L.; Ariza-Calderón, H.; Baños, L.; Perez-Bueno, J. J.; Rodríguez, M. E. Band gap energy determination by photoacoustic absorption and optical analysis of Cd1−xZnxTe for low zinc concentrations. *J. Cryst. Growth* **2006**, *286*, 279−283.
(55) Hof, M.; Hutterer, R.; Fidler, V. *Fluorescence Spectroscopy in Biology: Advanced Methods and Their Applications to Membranes, Proteins, DNA, and Cells*; Springer, 2005.
(56) Antaris, A. L.; Chen, H.; Diao, S.; Ma, Z.; Zhang, Z.; Zhu, S.; Wang, J.; Lozano, A. X.; Fan, Q.; Chew, L.; et al. A High Quantum Yield Molecule-protein Complex Fluorophore for Near-infrared II Imaging. *Nat. Commun.* **2017**, *8*, 15269.
(57) Takeda, Y.; Hayasaka, K.; Shiwaku, R.; Yokosawa, K.; Shiba, T.; Mamada, M.; Kumaki, D.; Fukuda, K.; Tokito, S. Fabrication of Ultra-Thin Printed Organic TFT CMOS Logic Circuits Optimized for Low-Voltage Wearable Sensor Applications. *Sci. Rep.* **2016**, *6*, 25714.


https://dx.doi.org/10.1021/acs.jpca.0c10567
J. Phys. Chem. A 2021, 125, 1870−1879